Modelling acoustic scattering by suspended flocculating sediments

Peter D. Thorne[1], Iain T. MacDonald[2] and Christopher E. Vincent[3]

1. National Oceanography Centre, Joseph Proudman Building, 6 Brownlow Street, Liverpool, L3 5DA, United Kingdom.

2. National Institute of Water and Atmospheric Research, Hamilton, Waikato, New Zealand.

3 School of Environmental Sciences,. University of East Anglia, Norwich, NR4 7TJ, United Kingdom.

*Corresponding author. Email: pdt@noc.ac.uk, Tel: +44 151 795 4862

N:\mydocuments\docw7\2014\flocs\re-submitted_text_figs.docx, pdf

Re-submitted 30/06/14

N:\mydocuments\docw7\2014\flocs\revised-manuscript.docx

N:\mydocuments\docw7\2014\flocs\revised-manuscript-marked.docx

Abstract

The development of a theoretical description of how sound interacts with flocculating sediments has been lacking and this deficiency has impeded sound being used to extract quantitative suspended sediment parameters in suspensions containing flocs. As a step towards theoretically examining this problem a relatively simple heuristic approach has been adopted to provide a description of the interaction of sound with suspensions that undergo flocculation. A model is presented for the interpretation of acoustic scattering from suspensions of fine sediments as they transition from primary particles, through an intermediate regime, to the case where low density flocs dominate the acoustic scattering. The approach is based on modified spherical elastic solid and elastic fluid scatterers and a combination of both. To evaluate the model the variation of density and compressional velocity within the flocs as they form and grow in size is required. The density can be estimated from previous studies; however, the velocity is unknown and is formulated here using a fluid mixture approach. Uncertainties in these parameters can have a significant effect on the predicted scattering characteristics and are therefore investigated in the present study. Further, to assess the proposed model, outputs are compared with recently published laboratory observations of acoustic scattering by flocculating cohesive suspensions.

Key words: Acoustic scattering, suspended cohesive sediments, flocculation, modelling, sediment transport.

List of main parameters and their units

a. Particle radius. (m)

a_o. Mean radius based on n(a). (m)

c_w. Sound velocity in water. (ms^{-1})

c_f. Sound velocity in a fluid scatterer. (ms^{-1})

c_s. Sound velocity in the primary particles. (ms^{-1})

C_f. Effective density flocculation constant. ($kgm^{(3-m)}$)

f. Intrinsic backscatter form function. (-)

f_{ss}. Intrinsic backscatter form function for a solid elastic sphere. (-)

f_{si}. Intrinsic backscatter form function for an irregularly shaped solid elastic particle. (-)

f_{fs}. Intrinsic backscatter form function for a fluid elastic sphere. (-)

f_{fi}. Intrinsic backscatter form function for an irregularly shaped fluid elastic scatterer. (-)

$f_{h.}$ Intrinsic hybrid backscatter form function for a scatter of variable density. (-)

f_o. Ensemble backscatter form function. (-)

f_{ho}. Ensemble hybrid backscatter form function for a scatter of variable density. (-)

k. Acoustic wavenumber, $2\pi/\lambda$. (m^{-1})

K. Sediment backscattering property. ($kg^{-1/2}m$)

m. Exponent to which the particle size is raised to parameterise flocculation.

M. The suspended concentration. (kgm^{-3})

n(a). Particle number radius probability density function. (-)

N. Number of particles per m^3 (m^{-3}).

r. Range from the transducer. (m)

$\mathfrak{R}$. The system constant. ($Vm^{3/2}$)

V. Root-mean-square backscattered signal. (V)

x=ka (-), x_o=ka_o (-)

α_w. Attenuation due to water absorption. (Nepers m^{-1})

α_s. Attenuation due to sediment scattering and viscous absportion. (Nepers m^{-1})

γ. Normalised density of the scatter relative to the density of water. (-)

γ_o. Minimum normalised density of the scatter relative to the density of water. (-)

δ. Normalised standard deviation σ/a_o of n(a). (-)

ε. Fluid heuristic formulation coefficients (-)

ζ. Normalised sound velocity of the scatter relative to the sound velocity in water. (-)

ζ_o. Minimum normalised sound velocity of the scatter relative to the sound velocity in water. (-)

κ_w. Compressibility of water. (Pa)

κ_s. Compressibility of the solid primary particles. (Pa)

λ. Wavelength of sound. (m)

υ. Kinematic viscosity (m^2s^{-1})

ξ. Sediment attenuation constant. ($kg^{-1}m^2$)

ρ_w. Density of water. (kgm^{-3})

ρ. Density of the suspended scatterers. (kgm^{-3})

ρ_s. Density of the solid primary particles. (kgm^{-3})

ρ_f. Density of a fluid scatterer. (kgm^{-3})

ρ_o. Minimum density of the suspended scatterers. (kgm^{-3})

ρ_e. Effective density of the suspended scatterers. (kgm^{-3})

σ. Standard deviation of n(a). (m)

φ. Porosity of the suspended scattterer.

χ. Intrinsic normalised total scattering cross-section. (-)

χ_{ss}. Intrinsic normalised total scattering cross-section for a solid elastic sphere. (-)

χ_{sv}. Intrinsic normalised total scattering cross-section for the viscous attenuation of a solid elastic sphere. (-)

χ_{fs}. Intrinsic normalised total scattering cross-section for a fluid elastic sphere. (-)

χ_{si}. Intrinsic normalised total scattering cross-section for an irregularly shaped solid elastic particle. (-)

χ_{fi}. Intrinsic normalised total scattering cross-section for an irregularly shaped fluid elastic scatterer. (-)

χ_h. Intrinsic hybrid normalised total cross-section for a scatter of variable density. (-)

χ_o. Ensemble normalised total scattering cross-section. (-)

χ_{ho}. Ensemble hybrid normalised total cross-section for a scatter of variable density. (-)

ψ. Transducer nearfield correction term. (-)

ω. Angular acoustic frequency. (s^{-1})

1. Introduction

The transport of sediments in coastal and estuarine waters is important because of the impact it has on aquatic habitats, water quality, turbidity, biogeochemistry and morphology (Amoudry and Souza, 2011). Developing capabilities to monitor and model marine sediment transport is therefore an essential component of coastal management (Davies and Thorne, 2008). To facilitate these developments new technologies are continually being investigated and acoustics is one of the techniques being used to advance our measurement capabilities (Thorne and Hay, 2012). Acoustics is being developed for sediment transport process studies because it is recognised as having the capability to measure non-intrusively, co-located, simultaneously and with high spatial-temporal resolution, suspended sediment (Pedocchi and Garcia, 2012) and flow profiles (Hurther and Thorne 2011) and provide information on bedforms (Hay, 2011).

The use of acoustics in non-cohesive inorganic sedimentary environments has been very successful, with many studies utilising sound to examine sediment transport processes over sandy beds (Hay et al, 2012; O'Hara Murray et al, 2012; Bolanos et al, 2012; Chassagneux and Hurther, 2014). In particular the acoustic approach has been successfully applied to the measurement of suspended sediments (Hay and Bowden, 1994; Thorne et al, 2009; O'Hara Murray et al, 2011). Apart from the technology developments, the success of the use of sound for suspension measurements has been due to an evolving description of the acoustic scattering properties of irregularly shaped sandy particles (Hay, 1991; Thorne and Meral, 2008; Moate and Thorne, 2013) and the development of inversion methodologies to extract suspension parameters from the backscattered sound (Crawford and Hay, 1993; Thosteson and Hanes, 1998; Hurther et al 2011, Moore et al 2013; Thorne and Hurther 2014). This has led to the development of multi-frequency acoustic backscatter systems for suspended sediment studies becoming available as commercial products and these are being utilised by the coastal and estuarine community.

Although acoustics has had success in measuring suspended sediments in regions predominantly composed of non-cohesive sandy sediments, its application in the regime of fine grained sediments, usually considered to be silts and clays, has been more problematic (Gartner, 2004; Ha et al, 2009; Ha et al, 2011; Sahin et al, 2013). When acoustic systems are used in studies on fine grained sediment transport, it is usually in combination with in-situ samples to calibrate and quantify the acoustic measurements (Shi et al, 1999; Holdaway et al; 1999; Fugate and Friedrichs, 2002; Moore et al, 2012), however, it is generally acknowledged that if the process of flocculation occurs during the measurement campaign, interpretation of the acoustic observations are challenging and uncertain. The main reason for this uncertainty arises because there has been neither measurements collected on the interaction of sound with flocculating sediments under controlled conditions, nor the development of a theoretical framework to describe such interactions. Therefore the use of multi-frequency acoustic backscatter systems to study sediment transport processes in cohesive fine grained environments is much less developed than that in the non-cohesive sandy regime.

To expand the quantitative use of acoustics, from non-cohesive sediments, to fine grained cohesive flocculating environments, a recent experimental study (MacDonald et al 2013) was carried out. In a series of acoustics backscatter measurements on suspensions of fine grained primary particles, of which flocs are composed, and, through the addition of a flocculating agent, on flocs formed by the aggregation of the primary particles, controlled acoustic observations were made on the interaction of sound with a suspension of flocculating sediments. As a complementary study to the experimental work, developments to model the observations have been in progress (Thorne et al, 2012a, b) and the result is reported here.

The methodology adopted for the flocculating scattering model is comparable to the heuristics approaches used in the description of non-cohesive sediment scattering (Hay, 1991; Schaafsma and Hay 1997; Thorne and Meral, 2008, Moate and Thorne, 2009) and zooplankton scattering (Johnson, 1977; Stanton 1990, Wiebe et al, 1990; Stanton and Chu, 2000). The concept is to utilise the acoustic scattering characteristic of well understood bodies with analytical solutions, such as spheres and cylinders, to form the basis of the scattering description, and modify, and often simplify, the analytical expressions to obtain formulae which can be usefully applied to more asymmetric irregularly shaped scattering bodies. This approach is well developed and used successfully in acoustics (Stanton and Chu 2000; Lawson et al, 2006; Thorne and Meral, 2008, Moate and Thorne, 2012). For the present study a modified solid elastic sphere is used to represent the scattering by primary particles and this has been validated with published data (Thorne and Meral, 2008). To represent the scattering characteristics of the somewhat nebulous collection of primary particles which compose a large low density floc, a single scattering body is proposed which has the combined acoustic properties of the water and the primary particles. A modified fluid elastic sphere model is used to characterise the scattering characteristics of the body using an approach similar to Johnson (1977). This fluid model was chosen because large flocculated scatterers have densities closer to that of water than the primary particles and would probably not sustain shear wave propagation. To obtain a description which covers the whole range from primary particles to low density flocs a hybrid model is proposed which provides continuous scattering behaviour based on the variation of particle density as the flocculation process occurs. To compare the scattering characteristics from such a hybrid model with observations, measured parameters from the experimental study of MacDonald et al (2013) are used to constrain the model output. Software to calculate floc scattering responses is given at http://noc.ac.uk/using-science/products/software/csr-acoustic-inversions Program name (3) - model_floc_paper.m.

2. Suspension scattering theory

2.1 Backscattered signal

The root-mean-square backscattered voltage, V, from an aqueous suspension of particles insonified using a disc transceiver, under conditions of incoherent scattering and when multiple scattering can be ignored (Sheng and Hay, 1988; Crawford and Hay, 1993; Thorne et al, 1993; Thorne and Hanes, 2002; Hurther et al, 2011) can be expressed as

$$V = \left(\frac{K\mathfrak{R}}{r\psi}\right) M^{1/2} e^{-2r(\alpha_w+\alpha_s)} \tag{1}$$

K represents the sediment backscattering properties, r is the range from the transceiver, ψ accounts for the departure from spherical spreading within the transducer nearfield (Downing et al 1995) and $\mathfrak{R}$ is the system constant (Betteridge et al 2008). The term α_ω is the sound attenuation due to water absorption and α_s is the attenuation due to suspended particle absorption and scattering. M is the suspended concentration and is based on the approximation $M \approx \frac{4\pi\rho(a_o)N}{3}\int_0^\infty a^3 n(a)da$, where N the number of scatterers per unit volume, $\rho(a_o)$ is the density of the scatterer and a_o is the suspension mean particle radius. The dependency of scatterer density on particles size is used to introduce the process of flocculation into the suspension scattering characteristics.

The scattering and attenuation terms can be formulated as follows

$$K = \frac{f_o}{(a_o\rho(a_o))^{1/2}}\,, \qquad \alpha_s = \frac{1}{r}\int_0^r \xi M\,dr\,, \qquad \xi = \frac{3\chi_o}{4a_o\,\rho(a_o)}$$

$$f_o(a_o) = \left[\frac{\int_0^\infty an(a)da\int_0^\infty a^2 f^2 n(a)da}{\int_0^\infty a^3 n(a)da}\right]^{1/2} \tag{2a}$$

$$\chi_o(a_o) = \frac{\int_0^\infty an(a)da\int_0^\infty a^2\chi n(a)da}{\int_0^\infty a^3 n(a)da} \tag{2b}$$

$$a_o = \int_0^\infty an(a)da \tag{2c}$$

f and χ are respectively the intrinsic form function and intrinsic normalised total scattering cross-section for the particles in suspension. Here intrinsic refers to the scattering characteristics measured using suspensions sieved into narrow size fractions. Physically, f describes the backscattering characteristics of a particle relative to its geometrical size, whilst χ quantifies the scattering from a particle over all angles, including viscous attenuation, relative to its cross-sectional area, and is proportional to attenuation. f_o and χ_o represent the ensemble mean scattering values obtained by integrating the intrinsic scattering characteristics over the particle size probability density function, n(a), of the particles in suspension.

2.2 Solid particle scattering characteristics

In their primary unflocculated state the primary particles can be considered as being solid elastic particles and represented using a modified sphere model. Such an approach has been used in a number of studies (Moate and Thorne, 2013). The intrinsic expressions for the backscatter form function and the normalised total scattering and viscous cross-section for a solid elastic sphere are given by

$$f_{ss} = \left| \frac{2}{ix} \sum_{n=0}^{\infty} (-1)^n (2n+1) b_n \right| \quad (3a)$$

$$\chi_{ss} = \frac{2}{x^2} \sum_{n=0}^{\infty} (2n+1) |b_n| \quad (3b)$$

$$\chi_{sv} = \frac{2}{3} x (\gamma - 1)^2 \frac{\tau}{\tau^2 + (\gamma + \theta)^2} \quad (3c)$$

Where

$$\tau = \frac{9}{4\beta a}\left(1 + \frac{1}{\beta a}\right), \quad \theta = \frac{1}{2}\left(1 + \frac{9}{2\beta a}\right)$$

The subscript 'ss' refers to solid sphere. In equations (3a) and (3b) b_n is a function containing spherical Bessel and Hankel functions and their derivatives, x=ka, where k=2π/λ, λ is the wavelength of the sound in water and a is the radius of the spheres in suspension (Faran,1951; Gaunaurd and Uberall, 1983; Thorne et al 1993 appendix and MacDonald et al 2013 Appendix A give b_n explicitly). The expression in equation (3c) (Urick 1948) accounts for viscous losses when for x<<1; $\gamma=\rho_s/\rho_w$ and $\beta=\sqrt{\omega/2\nu}$, where ω is the acoustic angular frequency, ν the kinematic viscosity for water, ρ_w is the density of water and ρ_s is the density of the solid particles. In the evaluation of ξ, $\chi= \chi_{ss}+ \chi_{sv}$. Figures 1a and 1b show the form of the expressions given in equation (3) for solid elastic spheres with shear and compressional velocities of c_{sh}=3545 ms^{-1} and c_s=5550 ms^{-1}, density of ρ_s=2600 kgm^{-3} and water properties of c_w =1480 ms^{-1}, ρ_w =1000 kgm^{-3}, ν=1.10^{-6} m^2s^{-1}.

Measurements (Hay, 1991; Schaafsma, and Hay, 1997; Moate and Thorne, 2009) have shown that for natural irregularly shaped sedimentary particles the detailed resonance structures associated with sharp dips in f_{ss} are not generally present due to the lack of symmetry in the shape of the particles and this allows simpler heuristic expressions to replace the relatively complex terms in equations (3a) and (3b). A number of similar intrinsic expressions have been published and the ones used here are based on a fit to a number of data sets (Thorne and Meral 2008) for suspensions of sands.

$$f_{si} = \frac{k_{sf}x^2\left(1-0.25e^{-((x-1.5)/0.5)^2}\right)\left(1+\ 0.35e^{-((x-2.0)/2.0)^2}\right)}{1.13+0.8k_{sf}x^2} \tag{4a}$$

$$\chi_{si} = \frac{k_{s\alpha}x^4}{1+x^2+\ 0.9k_{s\alpha}x^4} \tag{4b}$$

The subscript 'si' refers to solid irregular. Generally k_{sf} and $k_{s\alpha}$ are given by (Morse and Ingard, 1986)

$$k_{sf} = \frac{2}{3}\left|\eta_\kappa - \eta_\rho\right| \qquad k_{s\alpha} = \frac{4}{3}\left(\frac{\eta_\kappa^2+\eta_\rho^2/3}{6}\right)$$

$$\eta_\kappa = (\kappa_s-\kappa_w)/\ \kappa_w \qquad \eta_\rho = 3(\rho_s-\rho_w)/(2\rho_s+\ \rho_w)$$

κ_s and κ_w are respectively the compressibility for the solid particles in suspension and the surrounding water. Values used are κ_s=2.7.10^{-11} $Pa^{-1}$and κ_w=4.5.10^{-10} Pa^{-1} (Kay and Laby, 1986) which gives values of k_{sf} =1.15 and $k_{s\alpha}$ =0.24. The expressions for f_{si} and χ_{si} reduce to

x^2k_{sf} and $x^4k_{s\alpha}$ for $x<<1$, the Rayleigh scattering regime, and to a constant value generally greater than unity in the geometrical regime $x>>1$. In figures 1a and 1b the heuristic equations (4a) and (4b) are compared with the exact solutions of equations (3a) and (3b) where it can be seen that the results are comparable, though with the heuristic expressions lacking the resonance oscillations when $x>1$.

A number of measurements have been collected on scattering by inorganic non-cohesive sediments and these data are compared with the predictions in figure 1a and 1b. The solid circles in the figures are the mean of a number of measurements (Thorne and Meral 2008) and the crosses are from a series of studies summarised in Richards et al 2003. The comparisons show that equations (3c), (4a) and (4b) provide a reasonable description of scattering by solid elastic irregularly shaped particles. Therefore the non-cohesive elastic model given by equations (3c) and (4a) and 4(b) should represent the scattering characteristics of the elemental particles reasonably well.

2.3 Fluid particle scattering characteristics

When particles undergo flocculation the primary particles become loosely bound to form large fragile floc structures of dimensions tens to hundreds of times larger than the primary particles. These flocs are predominately composed of the water itself and are therefore not solid scatterers, but have densities close to water and easily shear apart. They could therefore be considered to have scattering characteristics closer to that of a fluid sphere rather than that of a solid elastic sphere. Considering flocs with densities much closer to that of water than the primary particles as fluid spheres, their intrinsic scattering characteristics can be expressed as (Anderson, 1950)

$$f_{fs} = \frac{2}{x}\left|\sum_{n=0}^{\infty}\frac{(-1)^n(2n+1)}{1+iC_n}\right| \qquad 5(a)$$

$$\chi_{fs} = \frac{2}{x^2}\sum_{n=0}^{\infty}\frac{(-1)^n(2n+1)}{1+C_n^2} \qquad (5b)$$

The subscript 'fs' refers to fluid sphere and C_n is composed of spherical Bessel and spherical Neumann functions (Anderson, 1950 equation (9) and MacDonald et al, 2013 Appendix A give C_n explicitly). Figure 1c and 1d show the form of the expressions given in equation (5) for fluid spheres having a compressional velocity of c_f=1.02c_w and a density of ρ_f=1.02ρ_w.

As with the primary particles, modified sphere heuristic expressions exist for the backscattering characteristics of irregular fluid scatterers (Stanton and Chu, 2000). Here the intrinsic backscatter form function uses a heuristic expression for a fluid sphere (Johnson (1977) which in the present study is modified to retain a form similar to equation (4a), though without the bracketed terms associated with solid particle oscillations.

$$f_{fi} = \frac{k_{ff} x^2}{1 + \varepsilon_1 x^2} \tag{6a}$$

The subscript 'fi' refers to fluid irregular. For the total normalise scattering cross-section a modified version of equation (4b) is used

$$\chi_{fi} = \frac{k_{f\alpha} x^4}{1 - \varepsilon_2 x + \varepsilon_3 x^2 + k_{f\alpha} x^4} \tag{6b}$$

Values selected for the coefficients ε_1, ε_2 and ε_3 were 1.2, 1.0 and 1.5 respectively. These values may well depend on floc structure and the degree of variability in the coefficients should be realised as experimental studies on floc scattering are carried out. This was the case for non-cohesive sediment acoustic scattering. Expressions for k_{ff} and $k_{f\alpha}$ (Clay and Medwin, 1997) are

$$k_{ff} = 2\left(\frac{\gamma\zeta^2 - 1}{3\gamma\zeta^2} + \frac{\gamma - 1}{2\gamma + 1}\right), \qquad k_{f\alpha} = 2\left(\left(\frac{\gamma\zeta^2 - 1}{3\gamma\zeta^2}\right)^2 + \frac{1}{3}\left(\frac{\gamma - 1}{2\gamma + 1}\right)^2\right)$$

The value for ζ is given by $\zeta = c_f/c_w$ and as before $\gamma = \rho_f/\rho_w$. The expressions for f_{fi} and χ_{fi} reduce to $x^2 k_{ff}$ and $x^4 k_{f\alpha}$ in the Rayleigh scattering regime. In figures 1c and 1d equations (6a) and (6b) are compared with equations (5a) and (5b) where it can be seen that the results are comparable, and, as with the solid scatters, the higher resonance oscillations are not present in the heuristic expressions. Unlike the case for solid elastic scatterers there are few measurements on fluid spheres (Hartog and Knollman, 1963) due to the difficulty in obtaining such measurements and none on irregularly shaped fluid bodies, although fluid sphere heuristic expressions have been applied successfully to acoustic scattering by zooplankton (Stanton 1989). The values selected for ε_1, ε_2 and ε_3 were found to give similar comparisons to those shown in figures 1c and 1d for a range of values for ζ and γ between 1.001-2.0.

2.4 Hybrid particle scattering characteristics

Equations (3c), (4a) and (4b) are considered to provide a description of the acoustic interaction with the solid primary particles and equations (6a) and (6b) have been suggested as expressions for scattering by low density fluid flocs. To link these two descriptions into a model that describes the scattering properties of the primary, transitional, and flocculated scatterers, the density and compressional velocity of sound in the scatterer are made a function of particle size. The term often used to indicate the degree of flocculation is the effective density, $\rho_e=\rho(a)-\rho_w$, where $\rho(a)$ is the floc density and ρ_e generally decreases as the floc size increases (Kranenburg, 1994; Fettweis, 2008; Manning et al 2007). The form for ρ_e with particle size is generally inverse linear on a log-log plot (Manning et al 2011) and can therefore be formulated as an inverse power of particle size (MacDonald et al, 2013)

$$\rho_e = \frac{C_f}{a^m} \tag{7}$$

The values of C_f $kgm^{(3-m)}$ and m vary depending on the process of flocculation (Manning et al 2011). As seen in the expressions above, equations (3c), (4) and (6), the density ratio between the scatterer and the fluid, $\gamma=\rho(a)/\rho_w$, is an important acoustic parameter for scattering and attenuation and using the expression for the effective density this can be written as

$$\gamma(a) = 1 + \frac{\rho_e}{\rho_w} \tag{8}$$

The other important ratio for scattering and attenuation is that of the sound velocity ratio in the scatterer to that in the fluid, $\zeta(a)=c(a)/c_w$. The velocity of sound within the flocs of a flocculating cohesive suspension has not been measured and is not known. To obtain an estimate for the compressional wave velocity in the flocs the approach adopted is based on the assumption that it has the same properties as that of a homogeneous fluid of the same mean density and compressibility. This approach was introduced by Wood (1930) for looking at fluid mixtures but it has also been applied to seabed porous sands (Hamilton, 1967). The water and solid components each contribute to the bulk compressibility and bulk density of the floc proportionally through the porosity of the mixture (Urick, 1947; Hamilton and Bachman, 1982; Buckingham, 1997). Using Wood's equation allows ζ to be expressed as

$$\zeta(\mathrm{a}) = \frac{1}{\mathrm{c_w}}(\{\phi\kappa_\mathrm{w} + (1-\phi)\kappa_\mathrm{s}\}\{\phi\rho_\mathrm{w} + (1-\phi)\rho_\mathrm{s}\})^{-1/2} \tag{9}$$

Here $\kappa_w=1/(\rho_w c_w^2)$, $\kappa_s=1/(\rho_s c_s^2)$ and ϕ is the porosity of the floc. Defining κ_s as equal to $1/(\rho_s c_s^2)$ is not strictly correct as $c_s^2 = (\kappa_s^{-1} + \frac{4}{3}G)/\rho_s$ for a solid, where G is the shear modulus, however, using $1/(\rho_s c_s^2)$ with the compressional velocity for the primary particles, provides the correct value for $\zeta(a)$ as $\phi \rightarrow 0$ and results in $k_{ff} \approx k_{sf}$ and $k_{f\alpha} \approx k_{s\alpha}$, thereby allowing equations 6(a) and 6(b) to also represent the primary particle scattering when x<<1. The porosity, ϕ, of the scatterer is given by

$$\phi = \frac{\rho_\mathrm{s} - \rho(\mathrm{a})}{\rho_\mathrm{s} - \rho_\mathrm{w}} \tag{10}$$

Using equations (3c), (6a) and (6b) with equations (7-10) provides a description for the suspension backscattering and attenuation characteristics of flocculation which transitions from solid scatterers, the primary particles, in the Rayleigh regime, through the intermediate region as flocs are formed, towards fluid scatterers as large low density flocs become dominant. For the modelling an upper value is placed on ρ_e such that $\rho_e \leq \rho_s - \rho_w$ and a lower imposed value of $\rho_e = \rho_o$. The former value is a physical restriction dictated by the grain density of the primary particles, while the latter is chosen as a minimum effective density.

3. Modelled flocculation scattering characteristics

3.1 Intrinsic floc scattering characteristic

To provide an illustration of the output from the scattering model for flocculating sediments an example is given in figure 2. The frequency used for the calculation was 3.0 MHz, this was chosen as it is a common acoustic frequency used in sediment process studies. The particle size varied from a=0.01-1000 μm, c_s=5550 ms^{-1}, ρ_s=2600 kgm^{-3}, c_w =1480 ms^{-1}, ρ_w =1000 kgm^{-3}, $\kappa_w=1/(\rho_w c_w^2)$, $\nu=1.10^{-6}$ m^2 s^{-1}, C_f=0.001 kgm^{-2} and m=1 (Manning et al 2011). For the solid irregular elastic scatter given by equation (4) $\kappa_s=2.7.10^{-11}$, while in equation (9) $\kappa_s=1/(\rho_s c_s^2)$. The elastic and acoustic properties of clay and silt sediments can be quite variable (Wang et al, 2001; Vanorio, 2003; Mondol et al, 2008) and the values used above are therefore indicative. In figure 2a the form for the effective density, $\rho_e(x)$ normalised by ρ_s-ρ_w is presented. Below 0.6 μm (x≈0.008) the effective density derived from equation (7) became greater than ρ_s-ρ_w and therefore the normalised value was set to unity. A minimum effective density of ρ_e=20 kgm^{-3} was applied, thereby yielding a minimum value for γ_o of 1.02. For the modelling an equivalent minimum value of 1.02 was also applied to ζ_o. This led to the forms for γ(x) and ζ(x) shown in figure 2a. It is the trends in γ(x) and ζ(x) with particle size that represents the process of flocculation in the scattering model.

In figure 2b is shown what would happen to the backscatter form function, f_{si}, calculated using equation (4a), if the irregular solid primary particles increased in diameter. This shows f_{si} increasing with x until around x≈2 where above this value f_{si} tends to a constant magnitude somewhat greater than unity. Also shown is the backscatter characteristics, calculated using equation (6a), f_{fi}, for an irregular fluid sphere with γ(x)= γ_o and ζ(x)= ζ_o. This shows a similar trend to the primary particles although with reduced values due to the much lower acoustic scattering characteristics. The solid line in figure 2b is the modelled hybrid intrinsic hybrid backscatter form function, f_h, as the scatterer transitions from a irregular solid elastic primary particle through a transition region to an irregular elastic fluid particle. This curve was calculated using equations (6a-10). The plot for f_h shows agreement with the f_{si} for the primary particles when x≤0.01 (a≤0.8 μm), f_h then progressively transitions from the primary scattering characteristics toward that of fluid scatterer, becoming essential fluid at x≈ 1 (a≈80 μm) and above this value f_h follows that of a fluid scatterer, f_{fi}, with scattering characteristics based on γ_o and ζ_o having a value of 1.02. In figure 2c results are shown for the normalised total scattering cross-section calculated using equations (3c, 4b, 6b-10). Similar trends are observed for χ_{si} and χ_{fi} below x≈1, although with χ_{fi} smaller in magnitude due to the lower scattering characteritsics. Above x≈1 χ_{si} tends to level off towards a value close to unity, while χ_{fi} tends to increase, though at a somewhat reduced rate. The further term in the normalised scattering cross-section is the viscous attenuation which begins to dominate attenuation when x $\lesssim$ 0.2 for the fluid sphere and x $\lesssim$ 0.1 for the solid sphere. A peak value in χ_{vi} is seen to occur at x≈0.01. As with figure 2b the solid line is the modelled hybrid intrinsic normalised total backscatter cross-section, χ_h, for a particle transitioning from a solid elastic primary particle, χ_{si}, through a transition region to an elastic fluid particle, χ_{fi}. As mentioned above χ_{sv} dominates below x $\lesssim$ 0.2 and in this regime χ_h follows the trend of χ_{sv}, above this value the attenuation due scattering begins to dominate and because the scattering characteristics have transitioned from solid to mainly fluid particle scattering by x≈0.2, χ_h is dominated by that of a fluid scatterer.

3.2 Ensemble floc scattering characteristics

The results presented in figure 2 are the intrinsic scattering characteristics and therefore represent scattering by a suspension with a very narrow particle size distribution. However, in practice marine suspensions typically have relatively broad size distribution. Therefore to obtain the ensemble scattering characteristics the intrinsic values need to be integrated over a size distribution, n(a), as defined in equations (2a) and (2b). The lognormal distribution is often used to describe the size probability density function of marine sediments (Soulsby, 1997) and is therefore used here with n(a) given by

$$n(a) = \frac{1}{a\mu_1\sqrt{2\pi}} e^{-(\log_e(a)-\mu_2)^2/2\mu_1^2} \tag{11}$$

$$\mu_1 = \sqrt{\log_e[\delta^2 + 1]}, \qquad \mu_2 = \log_e(a_o/\sqrt{1+\delta^2})$$

Where $\delta=\sigma/a_o$ is the normalised standard deviation and σ and a_o are respectively the standard deviation and mean of n(a). Figure 3 shows the impact on f_{ho} and χ_{ho} as the value for δ increased from 0.0 to 1.0. To obtain the plots equations (3c), (6a) and 6(b) were evaluated using equations (7-10) and integrating over n(a), given in equation (11), using equations (2a) and (2b) with a_o varying between 0.001-1000 μm. The parameters used to calculate the scattering characteristic were the same as those used in figure 2. The solid line, $\delta=0$, represents the intrinsic scattering characteristics and is identical to the solid line given in figure 2. Figure 3a shows the impact of increasing δ on f_{ho}, where it is observed that for $x_o<1$ the trend for f_{ho} is to increase with δ relative to f_h and with the increase being greater the smaller the value of x_o. For $x_o>1$, the trend is for f_{ho} to moderately reduce with δ relative to f_h with the reduction remaining nominally constant as x_o increases. Figure 3b shows the impact of increasing δ on χ. As can be seen in the figure the departure of χ_{ho} from χ_h increases with δ and this departure varies with x_o depending on the dominate attenuation term. These results clearly illustrate the impact δ can have on the ensemble scattering characteristics.

3.3 Model sensitivities

As mentioned above values for C_f and m in equation (7) are not unique and separate studies give different values depending on the sediment mineralogy and flocculation processes. To assess the impact variations in these two parameters had on the modelling of f_{ho} and χ_{ho} their values were changed and the results are shown in figure 4. In figure 4a the change in $\gamma(x)$ is shown for 20 different cases. The main impact is that as C_f and m increase the region over which the flocculation transition occur decreases, with the lower limit in x at which the scatterers reach the density of the primary particles increasing from $x=8.10^{-4}$ ($a=0.06$ μm) to $x=0.04$ ($a=3.0$ μm) for $C_f=0.0005$, $m=0.9$ and for $C_f=0.0015$, $m=1.1$ respectively. To assess the impact the changes in C_f and m had on the suspension scattering characteristics, f_{ho} and χ_{ho} were calculated using values identical with those used to obtain the plots in figures 2 and 3 with $\delta=0.5$. Taking $C_f=0.001$ and $m=1$ as a reference, the thick solid line in figures 4b and 4c, the plots show that in the transition region, $0.005\leq x_o \leq 1$, as C_f and m increases, the dashed lines, the values for f_{ho} and χ_{ho} increase, while if C_f and m decreases, the dotted lines, the values for f_{ho} and χ_{ho} decrease. These scattering changes are not marginal and lead to important differences in the modelled values for f_{ho} and χ_{ho} in the transition region.

In figure 5 comparisons are made of the modelled scattering characteristic as γ_o and ζ_o were varied between 1.005-1.3. All other parameters were the same as used to calculate the plots in figures 2 and 3 with $\delta=0.5$. In figure 5a the results for f_{ho} are shown. For values of $x_o\lesssim 0.01$ the impact of changes in γ_o and ζ_o on f_{ho} is negligible, between $x_o=0.01$-1 there is increasing divergence between the 20 curves and above $x_o\approx 1$ the values for f_{ho} remain nominally uniform, although for the $\gamma_o = \zeta_o=1.005$ case there is a slight reduction in values. The difference in the values for f_{ho} at x_o=10, between cases $\gamma_o = \zeta_o$=1.005 and $\gamma_o = \zeta_o$=1.3, is a factor of 40, indicating the impact γ_o and ζ_o have on the backscattering characteristic. The results for χ_{ho} are presented in figure 5b. In this case we can see that for $x \lesssim 0.05$ the variations in γ_o and ζ_o have little impact on χ_{ho}, above this value the 20 curves diverge with χ_{ho} taking on values of between 0.007- 0.6, at x_o=10, for γ_o and ζ_o having magnitudes over the range 1.005-1.3. As with the variation of the suspension scattering characteristic with C_f and m, changes in γ_o and ζ_o can lead to significant difference in the modelled values for f_{ho} and χ_{ho} as the larger flocs begin to dominate the scattering. The results presented in figures 3, 4 and 5 indicate that the modelled acoustics scattering characteristics of flocculating sediments are quite sensitive to the physical parameterisation of the flocculation process.

4. Comparison of the floc scattering model with measurements

The measurement of acoustic scattering by flocculating sediments is a difficult experiment to conduct and only recently has quantitative data been published (MacDonald et al, 2013). The objective of the study was to perform measurements on the scattering properties of the primary particles and by adding a flocculant to the primary suspension control the process of flocculation and measure the acoustic backscattered response. Details of the experimental study are given in MacDonald et al (2013) and only the salient features are outlined here for model comparison.

Acoustic backscatter measurements were carried out on suspensions of kaolin (Specwhite™ SiO_2 (47%), Al_2O_3 (38%), density 2600 kgm^{-3}) in a well-mixed re-circulation tank which generated a homogeneous suspension. Flocculation in the tank was controlled through the incremental addition of a commercial flocculent (MAGNAFLOC®). Mass concentrations between 0.2-3.2 kg m^{-3} were used and repeated measurements showed the kaolin was uniformly distributed to ±5% within the measurement region of the tank. Acoustic backscatter was measured using an Aquatec Aquascat-1000™ with transducers operating at frequencies of 3.0, 4.0 and 5.0 MHz over a range of 0.7 m at 0.01 m sampling intervals. The size distribution of the primary particles was determined using a Malvern MasterSizer 2000™. The floc size and settling velocity distributions for the flocculated suspension were determined using an optical FLOCView system. Figures 6a and 6b show measurements of the primary particles, and a representative floc size distribution, compared with lognormal probability density functions having a_o=0.43 μm, δ=0.85 and a_o=80 μm, δ=0.5 respectively. Over the size range of the flocs $\bar{\delta}$=0.5±0.2. Using the settling velocity and floc size with Stokes law allowed $\rho_e(a)$ to be estimated. The results were expressed in the form of equation (7) with C_f =5.83.10^{-4} and m=1.12. To obtain f_{ho} and χ_{ho} the approach of Thorne and Buckingham (2004) was adopted based on the assumption of a homogeneous concentration in the measurement tank and taking the natural logarithm of equation (1). It is the published values of f_{ho} and χ_{ho} with which the present model is compared.

To calculate the modelled scattering values for f_{ho} and χ_{ho} the following central parameters were used; ρ_s=2650 kg m^{-3}, ρ_w=1000 kg m^{-3}, c_s=2060 ms^{-1}, c_w=1480 ms^{-1}, ν=1.10^{-6} m^2s^{-1}, C_f =6.10^{-4}, m=1.1, (MacDonald et al, 2013), ε_1=1.4, ε_2=1.5, ε_3=1.0 and γ_o= ζ_o=1.05. The selection of c_s=2060 ms^{-1} is relatively low compared with some reported values (Wang et al, 2001; Vanorio, 2003; Mondol et al, 2008), however, the study of MacDonald et al (2013) indicated c_s=2060 ms^{-1} was the appropriate value to use for the comparison with their experimental data. As mentioned previously the ε coefficients will have a degree of uncertainty at this stage in the development of laboratory floc measurements and modelling, and were therefore selected pragmatically. Using equations (3c, 6-10) and integrating over n(a) using equation (2) with the lognormal distribution of equation (11) having δ(x) varying linearly from 0.85 for the primary particles to 0.5 for the low density flocs, f_{ho} and χ_{ho} were evaluated at 3.0, 4.0 and 5.0 MHz for a_o=0.001-1000 μm. To allow for uncertainties in the floc parameters the calculations were repeated at 4 MHz with C_f =3.10^{-4}, m=1.05, γ_o= ζ_o=1.025 and C_f =12.10^{-4}, m=1.2, and γ_o= ζ_o=1.1. These were not considered unreasonable uncertainties given the spread in the data used to estimate the floc parameters. The results of the modelling and the measured values for f_{ho} and χ_{ho} are shown in figure 7.

In figure 7a is shown the modelled values for f_{ho} at the three different frequencies using the central parameters and with the grey area indicating the region of uncertainty. The model shows steadily increasing values of f_{ho} with x_o for $x_o \lesssim 2$, with nominally uniform values of approximately 0.1 for x_o>2. Comparison of the model output with the primary particle observations, x_o<0.01, shows good agreement with the data with the model capturing the absolute level and trend of the solid primary particle scattering. The model marginally underestimates the measured values, however, the estimated region of uncertainty encompasses the data. For the floc measurements, x_o=0.5-3, a regime where fluid scattering becomes dominant in the model, the model captures the level of the measured values for f_{ho} and the increasing trend with x_o, although the data indicates f_{ho} increasing somewhat more steeply than modelled. This difference in steepness could be due to a number of factors including C_f and m not being invariant with a_o, n(a) having a somewhat different trend with a_o than that applied and the selected values for the ε coefficients in equation (6) may not be invariant with a_o. In figure 7b is shown the modelled values for χ_{ho} which show a somewhat different form with x_o to that of f_{ho}. For values of $x_o \lesssim 0.1$ the dominant component of χ_{ho} is associated with viscous attenuation, this is seen to steadily increase initially with x_o peaking at a value of $\chi_{ho} \approx 5.10^{-4}$ at $x_o \approx 0.01$ and thereafter declining due to the reducing particle density. Above $x_o \approx 0.1$, the fluid scattering component of χ_{ho} begins to prevail and steadily increases with x_o. Comparing the model with the observations for the solid primary particle regime, the modelled values for χ_{ho} are comparable in level and form with the data. The measurements of χ_{ho} shown in figure 7b for the primary particles have relatively large error bars due to experimental difficulties in obtaining accurate values for χ_{ho} when attenuation due to water absorption is comparable with the suspension attenuation (Moate and Thorne 2009). In the regime of floc scattering, x_o=0.5-3, the model is dominated by the fluid particle scattering characteristics and is seen to follow the data reasonably well both in terms of magnitude and trend. There is some underestimate of the absolute level and this could be associated with the factors noted above in the difference in steepness for f_{ho}, although, generally, the data lie within the region of estimated uncertainty. The model therefore captures in broad terms the general behaviour of the observed primary and flocculated scattering characteristics.

5. Conclusions

The use of acoustics to study suspended sediment transport processes, in environments of non-cohesive inorganic sandy sediments, has developed significantly over the past two to three decades. Underpinning the use of the acoustic technology has been the development of a comprehensive theory on the interaction of sound with suspensions of irregularly shaped scatterers. These theoretical developments have been assessed using data from a number of experimental studies. With the veracity of the scattering theory established for non-cohesive sediments, it has been possible to develop inversion methodologies, to extract suspension parameters, using the signal backscattered from suspended sediments in the marine environment. It has been this combination of technology advancement, theoretical developments and inversion methodologies, which has led to the increasing application of acoustics in the study of non-cohesive sediment transport processes (Thorne and Hay 2012).

Although acoustics has had success in its application over non-cohesive sandy beds, its utility in cohesive silt and clay environments, where flocculation can occur, has been much more challenging. The primary reason for this difficulty has been the lack of experimental data and a theoretical framework for the interpretation of the backscattered signal from flocculating suspensions. This has resulted in the analysis of acoustic measurements of cohesive suspension processes being much more problematic than that of non-cohesive. To investigate the scattering characteristics of primary particles and flocculating cohesive sediments a laboratory study was conducted and the results recently published (MacDonald et al, 2013). In complementary studies (Thorne et al, 2012a,b), aimed at developing a model of the acoustic scattering characteristics of suspended cohesive sediments, an approach using heuristic formulations based on spherical scatterers was proposed. Such a heuristic approach has often been used in underwater acoustics to study complex shaped scattering bodies (Stanton and Chu, 2000; Thorne and Meral; 2008). In the present study a modified solid elastic sphere has been used to describe the scattering of the primary particles and a modified fluid elastic scatter to characterise the scattering of large low density flocs. To link these two descriptions together a hybrid model has been proposed based on variable particle density to represent the processes of flocculation. This variable density has been used with Woods equation to obtain the compressional sound velocity in the flocs and thereby their acoustic scattering characteristics. The aim of the model was to describe the scattering characteristics of the primary micron size sediments through the transition process of flocculation, to large low density flocs. To examine the model comparisons were made with recently published data (MacDonald et al, 2013). The output from the model captured the observations reasonably well, considering the lack of detailed internal floc structure incorporated into the heuristic hybrid model. To accommodate the internal structure of flocs into a description of their scattering characteristics, theories such as those of Biot 1956a, 1956b, 1962 and the more recent works of Buckingham 1997, 1998, 2000, 2005 and 2007 could be considered. These provide a more detailed description of the interaction of sound with an aqueous porous body composed of marine sediments and may therefore have application to floc scattering.

The model presented here compared reasonably well with the measurements from the laboratory study, where conditions were well prescribed and parameters carefully measured. However, the results in figures 3-5 show that scattering characteristic can have significantly different values depending on the input values to the model. Changes in C_f, m, ζ, γ, ρ_s, c_s, n(a) and the coefficients in equation (6) all impact on the modelled acoustic scattering of flocculating sediments. Therefore the application of the model to field studies has to be carried out judiciously, with as many supporting measurements as practicable to constrain the input parameters and with outputs calculated using reasonable variability on the inputs to establish the veracity of the model output.

If acoustics is to be used quantitatively in flocculating marine sediment process studies, then a description of the acoustic scattering processes is required, coupled with an inversion algorithm to extract suspension parameters. The model presented here is considered to be a step towards this goal. To-date only one controlled experiment on the acoustic interaction with flocculating sediment has been reported, with a flocculation region between x_o=0.5-3.0. There is a broad region, roughly between x_o=0.01-0.5 which was not covered in the experimental study. Therefore there is a definite requirement for further well controlled laboratory studies on acoustic scattering with suspension of flocculating sediments. This will enable the present and any other developing theoretical models to be assessed and advanced. It is anticipated that such measurements and modelling will broaden the application of the quantitative application of acoustic into the complex regime of flocculating sediments.

Acknowledgments

This work was supported by the National Environmental Research Council, UK, research grants FLOCSAM, COHBED, EU Hydralab JRA WISE and NOC national capability funds. Dr Benjamin D. Moate is thanked for his contributions to the acoustic system calibration and discussions on acoustic scattering by marine suspensions. The reviewers are also thanked for their useful comments and suggestions.

REFERENCES

Amoudry, L. O., and Souza A.J., 2011. Deterministic coastal morphological and sediment transport modeling: A review and discussion, Rev. Geophys., 49, RG2002, doi:10.1029/2010RG000341.

Anderson V.C, 1950. Sound scattering from a fluid sphere," J. Acoust. Soc. Am. 22, 426-431.

Betteridge, K.F.E., Thorne, P.D. and Cooke, R.D., 2008. Calibrating multi-frequency acoustic backscatter systems for studying near-bed suspended sediment transport processes. Continental Shelf Research., 28, 227-235.

Biot M. A. 1956a. Theory of propagation of elastic waves in a fluid-saturated porous solid. I. Low-frequency range. J. Acoust. Soc. Am. 28, 168–178.

Biot, M. A. 1956b. Theory of propagation of elastic waves in a fluid-saturated porous solid. II. Higher frequency range. J. Acoust. Soc. Am. 28, 179–191.

Biot M. A. 1962. Mechanics of deformation and acoustic propagation in porousmedia. J. Appl. Phys. **33**, 1482–1498.

Bolanos R, Thorne PD and Wolf J. 2012.Comparison of measurements and models of bed stress, bedforms and suspended sediments under combined currents and waves. Coastal Engineering 62, 19-30.

Buckingham M.J., 1997. Theory of acoustic attenuation, dispersion, and pulse propagation in unconsolidated granular materials including marine sands. J. Acoust. Soc. Am. 102 (5), 2579-2576.

Buckingham M. J. 1998. Theory of compressional and shear waves in fluid like marine sediments. J. Acoust. Soc. Am. **103**, 288–299.

Buckingham M. J. 2000. Wave propagation, stress relaxation, and grain-to grain shearing in saturated, unconsolidated marine sediments. J. Acoust. Soc. Am. 108, 2796–2815.

Buckingham M. J. 2005. Compressional and shear wave properties of marine sediments: Comparisons between theory and data. J. Acoust. Soc. Am. 117, 137–152.

Buckingham M. J. 2007. On pore-fluid viscosity and the wave properties of saturated granular materials including marine sediments. J. Acoust. Soc. Am. 122, 1486–1501.

Chassagneux, F. X., and D. Hurther 2014, Wave bottom boundary layer processes below irregular surfzone breaking waves with light-weight sheet flow particle transport, J. Geophys. Res. Oceans, 119, doi:10.1002/ 2013JC009338.

Clay C.S. and Medwin H. 1997. Acoustical Oceanography. A Wiley-Interscience publication, New York. Chapter 6.

Crawford, A.M., Hay, A.E., 1993. Determining suspended sand size and concentration from multifrequency acoustic backscatter. J. Acoust. Soc. Am. 94 (6), 3312-3324.

Davies A. G. and Thorne P.D. 2008. Advances in the study of moving sediments and evolving seabeds. Surveys in Geophysics Vol 29, No 1, January, 1-36.

Downing, A., Thorne, P.D. and Vincent, C.E., 1995. Backscattering from a suspension in the near field of a piston transducer. Journal Acoustical Society of America, 97 (3), 1614-1620.

Faran J.J. 1951. Sound scattering by solid cylinders and spheres. Journal Acoustical Society of America. Vol. 23 (4) 405-418.

Fettweis M., 2008. Uncertainty of excess density and settling velocity of mud flocs derived from in situ measurements. Estuarine, Coastal and Shelf Science, 78, 426-436.

Fugate D.C. and Friedrichs C.T., 2002. Determining concentration and fall velocity of estuarine particle populations using ADV, OBS and LISST. Continental Shelf Research 22, 1867–1886.

Gartner J. W. (2004). Estimating suspended solids concentrations from backscatter ntensity measured by acoustic Doppler current profiler in San Francisco Bay, California. Marine Geology 211 (2004) 169–187.

Gaunaurd G. C. and Uberall H. 1983. RST analysis of monostatic and bistatic acoustic echoes from an elastic sphere. Journal Acoustic Society of America Vol. 73 (1) 1-12.

Ha H.K., Hsu W.Y., Maa J.P.Y, Shao Y.Y., and Holland, C.W., 2009. Using ADV backscatter strength for measuring suspended cohesive sediment concentration. Continental Shelf Research 29, 1310–1316.

Ha H.K, Maa J.P.Y, Park K, and Kim Y.H., 2011. Estimation of high-resolution sediment concentration profiles in bottom boundary layer using pulse-coherent acoustic Doppler current profilers. Marine Geology 279 (2011) 199–209.

Hamilton E.L. and Bachman R.T., 1982. Sound velocity and related properties of marine sediments. J. Acoust. Soc. Am. 72 (6), 1891-1904.

Hampton L. D., 1967. Acoustic properties of sediments. J. Acoust. Soc. Am. 42 (4), 882-890.

Hartog J. J. and Knollman G. C, 1963. Measurements of underwater sound scattered from a fluid sphere. J. Acoust. Soc. Am. 35 (4), 538-541.

Hay, A.E., 1991. Sound scattering from a particle-laden turbulent jet, J. Acoust. Soc. Am., 90, 2055-2074.

Hay, A.E., and Bowen, A.J., 1994. Coherence scales of wave-induced suspended sand concentration fluctuations. Journal of Geophysical Research 99 (C6), 12749–12765. doi:10.1029/94JC00290.

Hay A. E., 2011. Geometric bottom roughness and the bed state storm cycle. Journal of Geophysical Research, 116. C04017, doi:1029/2010JC006687.

Hay A. E., Zedel L., Cheel R. and Dillon J., 2012. On the vertical and temporal structure of flow and stress within the turbulent oscillatory boundary layer above evolving beds. Continental Shelf Research, 46, 31-49.

Holdaway, G.P., Thorne, P.D., Flatt, D., Jones, S.E., Prandle, D., 1999. Comparison between ADCP and transmissometer measurements of suspended sediment concentration. Continental Shelf Research 19, 421–441.

Hurther D. and Thorne P.D. 2011. Suspension and near-bed load sediment transport processes above a migrating, sand-rippled bed under shoaling waves. J. Geophys. Res., Vol 116, C07001, doi:1029/2010JC006774.

Hurther, D, Thorne, PD and Bricault M, Lemmin U and Baroud JM. 2011. A multi-frequency acoustic concentration and velocity profiler (ACVP) for boundary layer measurements of fine-scale flow and sediment transport processes. Coastal Engineering. 58, 294-605 doi: 10.1016/j.coastaleng.2011.01.006.

Johnson, R. K. 1977. Sound scattering from a fluid sphere revisited. Journal of the Acoustical Society of America, 62. 375–377; ‘‘Erratum: ‘Sound scattering from a fluid sphererevisited’.’’ Journal of the Acoustical Society of America, 63, 626 (1978).

Kaye G. W. C and Laby T. H. 1986. Tables of Physical and Chemical Constants. Published by Longman Group Limited.

Kranenburg C, 1994. The fractal structure of cohesive sediment aggregates. Estuarine, Coastal and Shelf Sciences, 39, 451-460.

Lawson, G.L., P.H. Wiebe, C.J. Ashjian, D. Chu, and T.K. Stanton, 2006. Improved parameterization of Antarctic krill target strength models. J. Acoust. Soc. Am.119 (1), 232-242.

MacDonald IT, Vincent CE, Thorne P.D. and Moate PD. 2013. Acoustic scattering from a suspension of flocculated sediments. J. Geophysical Research: Oceans, Vol 118, 1-14, doi:10.1002/jgrc.20197, 2013.

Manning A.J., Friend P.L., Prowse N and Amos C.L, 2007. Estuarine mud flocculation properties determined using an annular mini-flume and the LabSFLOC system. 27, 1080-1095

Manning, A.J., Baugh, J.V., Soulsby, R.L., Spearman, J.R. and Whitehouse, R.J.S. (2011). Cohesive Sediment Flocculation and the Application to Settling Flux Modelling. In: Dr. Silvia Susana Ginsberg (Ed.), Sediment Transport, Publisher: InTech (Vienna), Chapter 5, pp. 91-116, DOI: org/10.5772/16055, ISBN: 978-953-307-189-3. Available from: http://www.intechopen.com/books/sediment-transport/cohesive-sediment-flocculation-and-the-application-to-settling-flux-modelling

Moate B. D. and Thorne P. D., 2009. Measurements and inversion of acoustic scattering from suspensions having broad size distributions. Journal Acoustical Society America, 126(6), 2905-1917.

Moate BD and Thorne PD. 2012. Interpreting acoustic backscatter from suspended sediments of different and mixed mineralogical composition. Continental Shelf Research. Continental Shelf Research, 46, 67-82.

Moate B.D. and Thorne P.D., 2013. Scattering from suspended sediments having different and mixed mineralogical compositions: Comparision of laboratory measurements and theoretical predictions. Journal Acoustical Society America 133(3) 1320-1334.

Moore, S. A., Le Coz J., Hurther D. and Paquier A. 2012. On the application of horizontal ADCPs to suspended sediment transport surveys in rivers. Continental Shelf Research, 46, 50-63.

Moore, S. A., Le Coz, J., Hurther, D., & Paquier, A. (2013). Using multi-frequency acoustic attenuation to monitor grain size and concentration of suspended sediment in rivers. Journal of the Acoustical Society of America, 133(4), 1959–1970.

Mondol N.H., Jahren J, and Bjorlykke K, 2008. Elastic properties of clay minerals. The Leading Edge, June, 758-770.

Morse P. M. And Ingard K.U. 1986. Theoretical Acoustics. Published by Princeton University Press, Princeton, New Jersey. Chap 8.

O'Hara Murray, R. B., Thorne, PD and Hodgson DM. 2011. Intrawave observations of sediment entrainment processes above sand ripples under irregular waves, J. Geophys. Res., 116, C01001, doi:10.1029/2010JC006216.

O'Hara Murray, Hodgson D.M. and Thorne P.D., 2012. Wave groups and the character of sediment resuspension over an evolving sandy bedforms. Continental Shelf Research, 46, 16-30.

Pedocchi F, and Garcia M. H. 2012. Acoustic measurement of suspended sediment concentration profiles in an oscillatory boundary layer. Continental Shelf Research, 46, 87-95.

Richards S.D., Leighton T.G. and Brown N.R., 2003. Visco-inertial absorption in dilute suspensions of irregular particles. Proceedings of the Royal Society London, 459, 2153-2167.

Sahin C, Safak I, Hsu T.J. and Sheremet A, 2013. Observations of suspended sediment stratification from acoustic backscatter in muddy environments. Marine Geology 336 24–32

Schaafsma A. S. and Hay A. E. 1997. Attenuation in suspensions of irregularly shaped sediment particles: A two-parameter equivalent spherical scatterer model. Journal Acoustical. Society of America. 102, 1485-1502.

Sheng, J. and Hay, A.E., 1988. An examination of the spherical scatterer approximation in aqueous suspensions of sand, J. Acoust. Soc. Am., **83**: 598–610.

Shi Z, Ren L.F. and Hamilton L.J, 1999. Acoustic profiling of fine suspension concentration in the Changjiang Estuary. Estuaries, 22, 3A, 648-656

Soulsby, R.L., 1997. Dynamics of Marine Sands. A Manual for Practical Applications. Thomas Telford publications, London, UK.

Stanton, T.K, 1989. Simple approximate formulas for backscattering of sound by spherical and elongated objects, J. Acoust. Soc. Am. 86 (4), 1499-1510.

Stanton TK, 1990. Sound scattering by spherical and elongated shelled bodies. J. Acoust. Soc. Am. 88 (3), September 1619-1633.

Stanton T.K and Chu D, 2000. Review and recommendations for the modelling of acousticscattering byfluid -like elongated zooplankton: euphausiids and copepods. ICES Journal of Marine Science, 57: 793–807.

Thorne, P.D., Hardcastle, P.J., and Soulsby, R.L., 1993. Analysis of acoustic measurements of suspended sediments. Journal of Geophysical Research, 98 (C1), 899-910.

Thorne, P.D. and Hanes, D.M., 2002. A review of acoustic measurement of small-scale sediment processes. Cont. Shelf Res., 22, 603-632.

Thorne, P.D. and Buckingham, M.J., 2004. Measurements of scattering by suspensions of irregularly shaped sand particles and comparison with a single parameter modified sphere model. Journal of the Acoustical Society of America, 116 (5), 2876-2889.

Thorne, P.D. and Meral, R., 2008. Formulations for the scattering properties of sandy sediments for use in the application of acoustics to sediment transport. Journal of Continental Research, 28, 309-317.

Thorne P. D., A. G. Davies, and P. S. Bell 2009. Observations and analysis of sediment diffusivity profiles over sandy rippled beds under waves, J. Geophys. Res., 114, C02023, doi:10.1029/2008JC004944.

Thorne P. D. and Hay A.E. 2012. Introduction to the special issue of Continental Shelf Research; On the application of acoustics to sediment transport processes. Continental Shelf Research, 46, 1.

Thorne PD, Moate BD and MacDonald IT. 2012a. A tentative model for acoustic scattering by flocculating suspended sediments. In the proceedings of the 11th European Conference on Underwater Acoustics CD-rom, held in Edinburgh, UK 2-6 July 2012. Vol 34. Pt.3.2012. ISBN 978-1-906913-13-7.ISSN 1467-6095.102-107.

Thorne PD, MacDonald IT, Moate BD and Vincent CE. 2012b. Acoustic scattering by flocculating suspended sediments: A provisional model. Published in PiE2012. Particles in Europe, ICM, Barcelona, Spain. 17-19 October 2012. Program and Abstract Volume. 112-115.

Thorne P.D. and Hurther D. 2014. An Overview on the use of backscattered sound for measuring suspended particle size and concentration profiles in non-cohesive inorganic sediment transport studies. Continental Shelf Research. 73, 97-118.

Thosteson, E. D. Hanes D. M. 1998 A simplified method for determining sediment size and concentration from multiple frequency acoustic backscatter measurements", J. Acoust Soc Am. 104(2), 820-830.

Urick R.J, 1947. A sound velocity method for determining compressibility of finely divided substances. J. Appl. Phys 18, 983-987.

Urick R.J, 1948. The absorption of sound in suspensions of irregular particles. J. Acoust Soc. Am. 20,3 283-289.

Vanorio T, Prasad M and Nur A, 2003. Elastic properties of dry clay mineral aggregates, suspensions and sandstones. Geophys J. Int, 155, 319-326.

Wiebe, P.H., C.H. Greene, T.K. Stanton, and J. Burczynski, 1990. Sound scattering by live zooplankton and micronekton: Empirical studies with a dual beam acoustical system. J. Acoust. Soc. Am.88 (5), 2346-2360.

Wood A. B., 1930. A textbook of sound. G. Bell and Son.

Wang Z.Z, Wang H and Cates M.E, 2001. Effective elastic properties of solid clay. Geophysics, 66 (2), 428-440.

FIGURE CAPTIONS

Figure 1. Theoretical comparisons of sphere and heuristic intrinsic form function, f, and intrinsic normalised total scattering cross-section, χ. Equations used are given by the numbers in the brackets in the legend, see text for the equations. Measurements are presented from Thorne and Meral, 2008 (●) and Richards et al, 2003 (x) for solid scatters. a) and b) are for a solid scatterer and c) and d) are for a fluid scatter.

Figure 2. Calculations for a) the normalised effective density, $\rho_e/(\rho_s-\rho_w)$, density ratio, γ, and velocity ratio, ζ, b) the intrinsic form function, f, and c) the intrinsic normalised total scattering cross-section, χ, for a solid, fluid and hybrid scatterer. Equation numbers are given in brackets in the legend, see text for the equations.

Figure 3. Calculations for a) the hybrid ensemble form function, f_{ho}, and b) the hybrid ensemble normalised total scattering cross-section, χ_{ho}, with increasing normalised standard deviation, δ, for a lognormal particle size probability density function, n(a).

Figure 4. Variation of a) the normalised density of the scatterer, γ, with C_f and m and the impact this has on b) the hybrid ensemble form function, f_{ho}, and c) the hybrid ensemble normalised total scattering cross-section, χ_{ho}. The lines represent C_f>0.001 and m>1.0 (— —), C_f<0.001 and m<1.0 (· · ·) and C_f=0.001 and m=1.0 (▬).

Figure 5. Variation of a) the hybrid ensemble form function, f_{ho}, and b) the hybrid ensemble normalised total scattering cross-section, χ_{ho}, with the lower limit of the density, γ_o, and velocity ratios set equal to $\zeta_o = \gamma_o$=1.005-1.3.

Figure 6. Lognormal particle size probability density function fits (—) to measurements (●) for; a) the primary particles and b) an example for the flocs.

Figure 7. Comparison of the model output with the measurements. In the legend for the measurements P refers to primary particles, F to flocs and the subscript is the acoustic frequency in megahertz. The three lines are the modelled scattering characteristics at 3.0 MHz (— —), 4.0 MHz (—) and 5.0 MHz (— • —) using the central parameters, see text, with the grey region associated with uncertainties in the floc parameters, see text.

n:\mat5work\sizescatter\comp_se_sf_models2_b.m

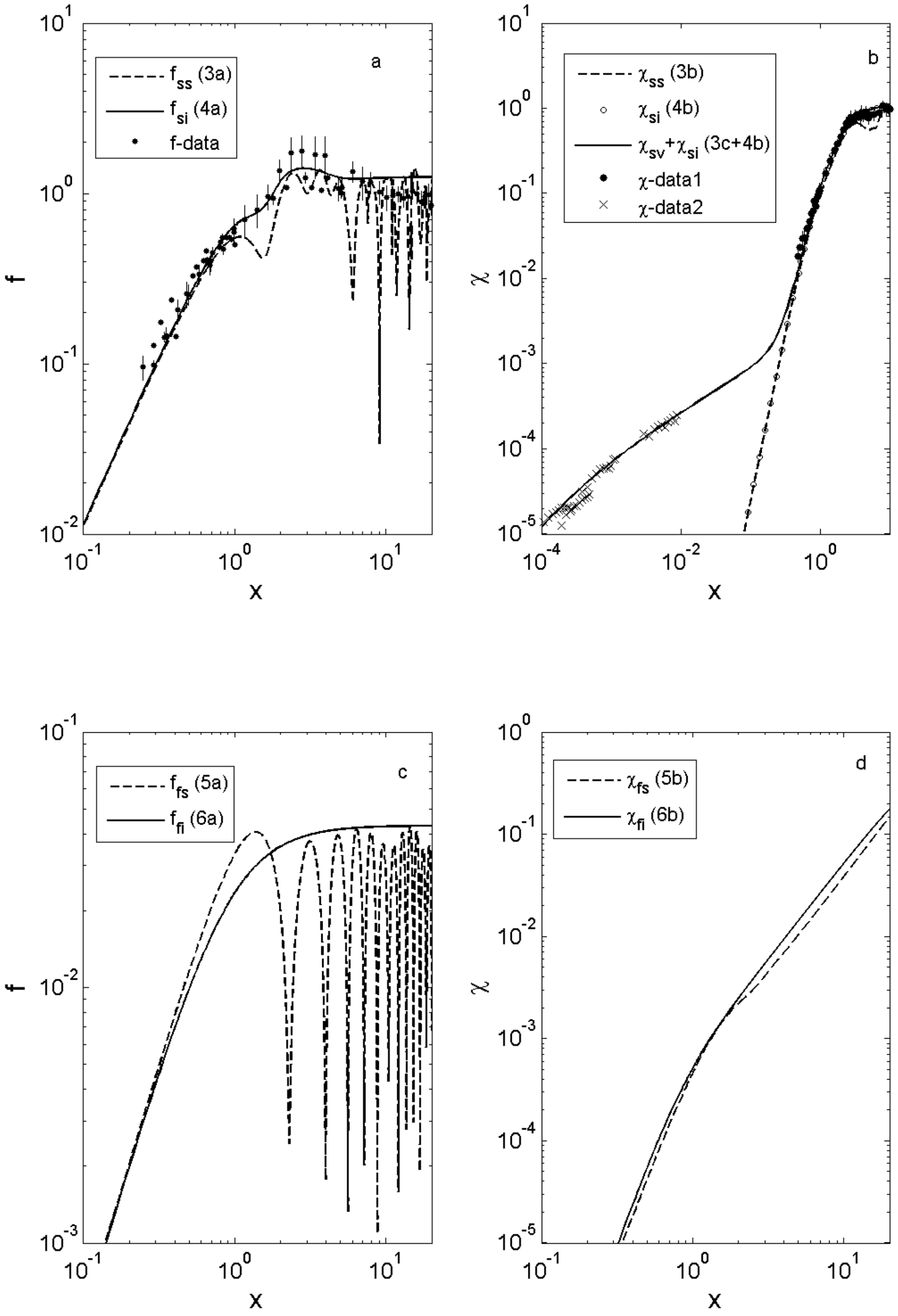

Fig 1.

n:\mat5work\sizescatter\floc\model_singlesizeb2.m

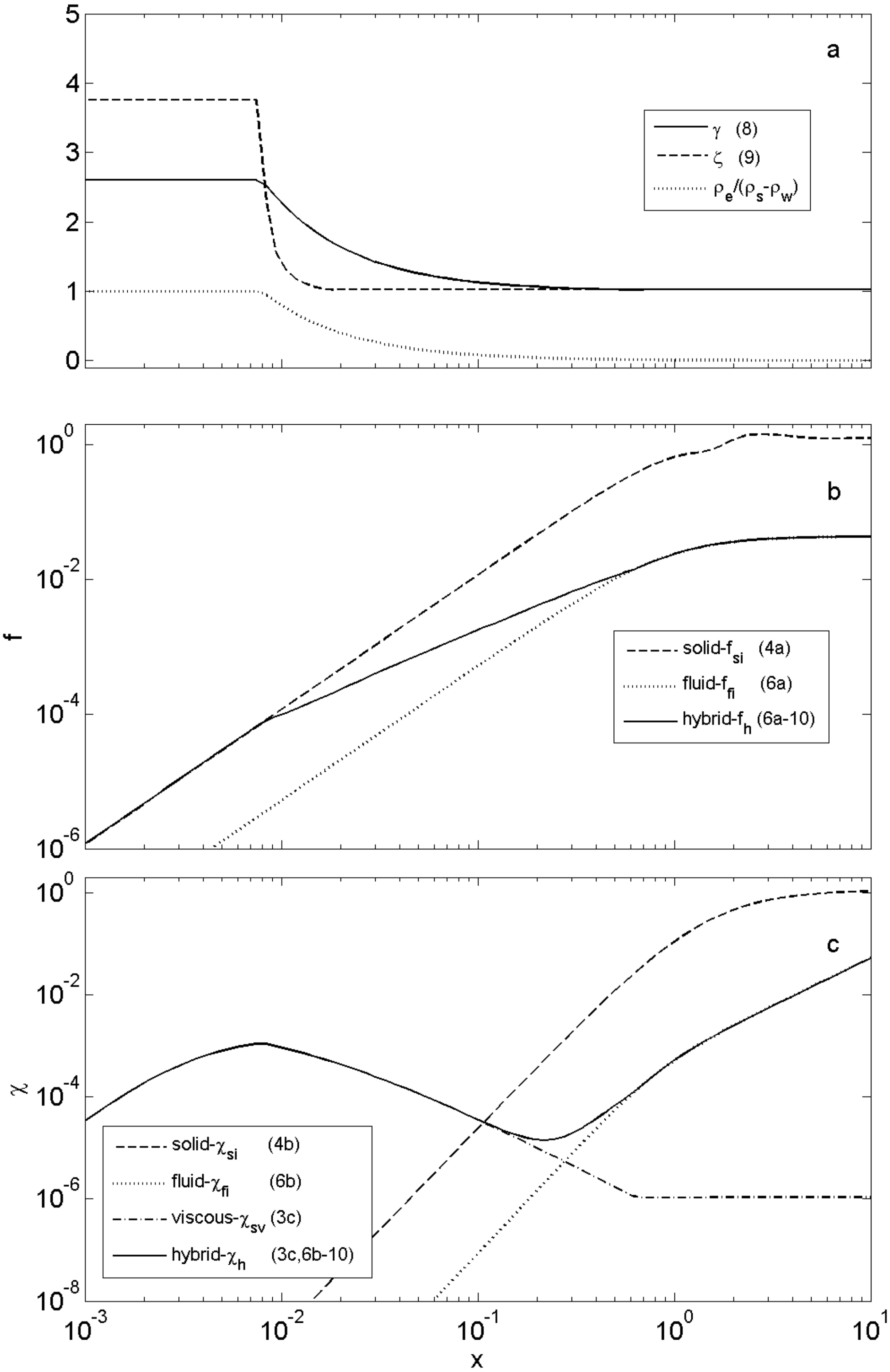

Fig 2.

n:\mat5work\sizescatter\floc\model_avesizeb2.m

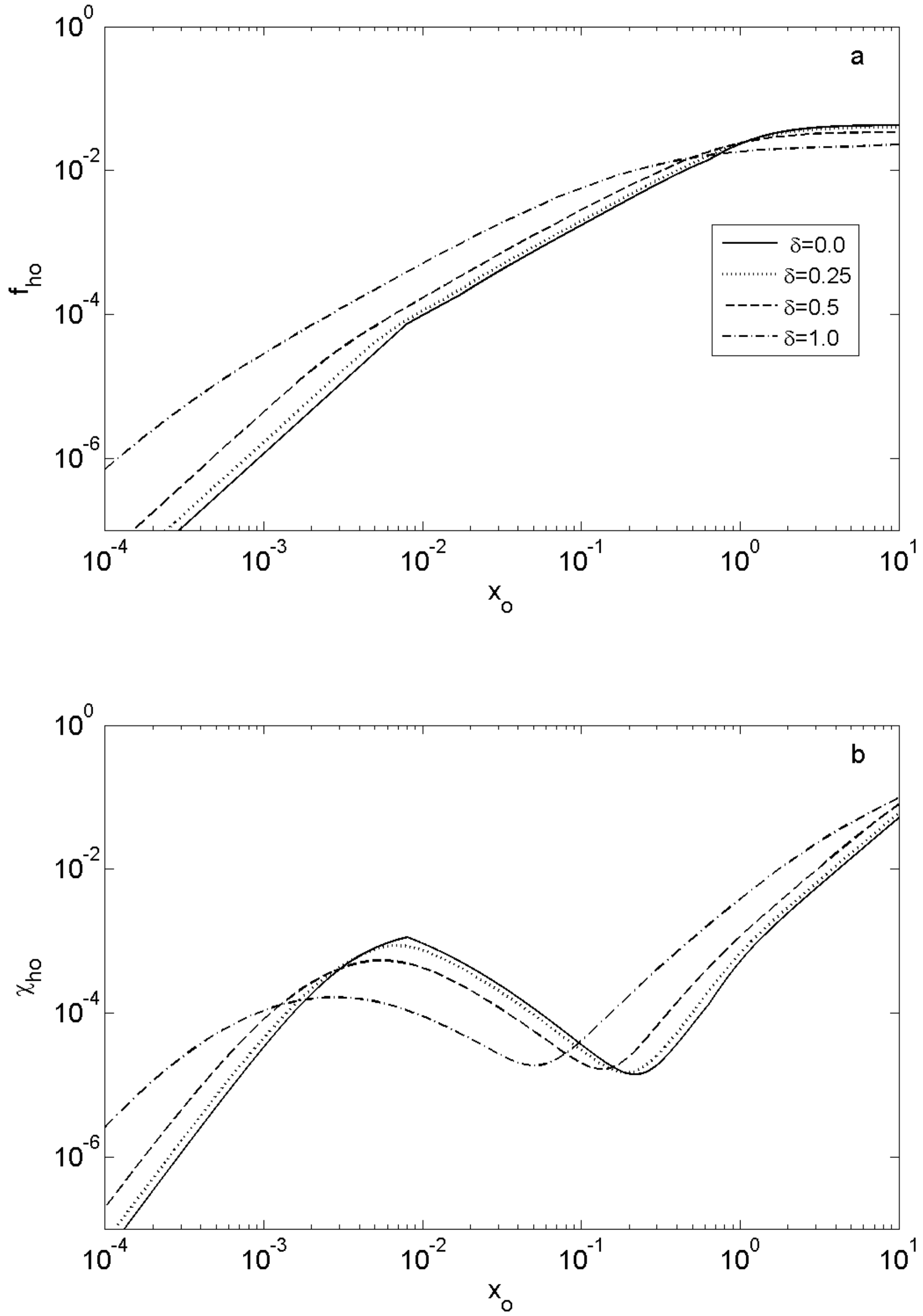

Fig 3.

n:\mat5work\sizescatter\floc\model_avesizec2_b.m

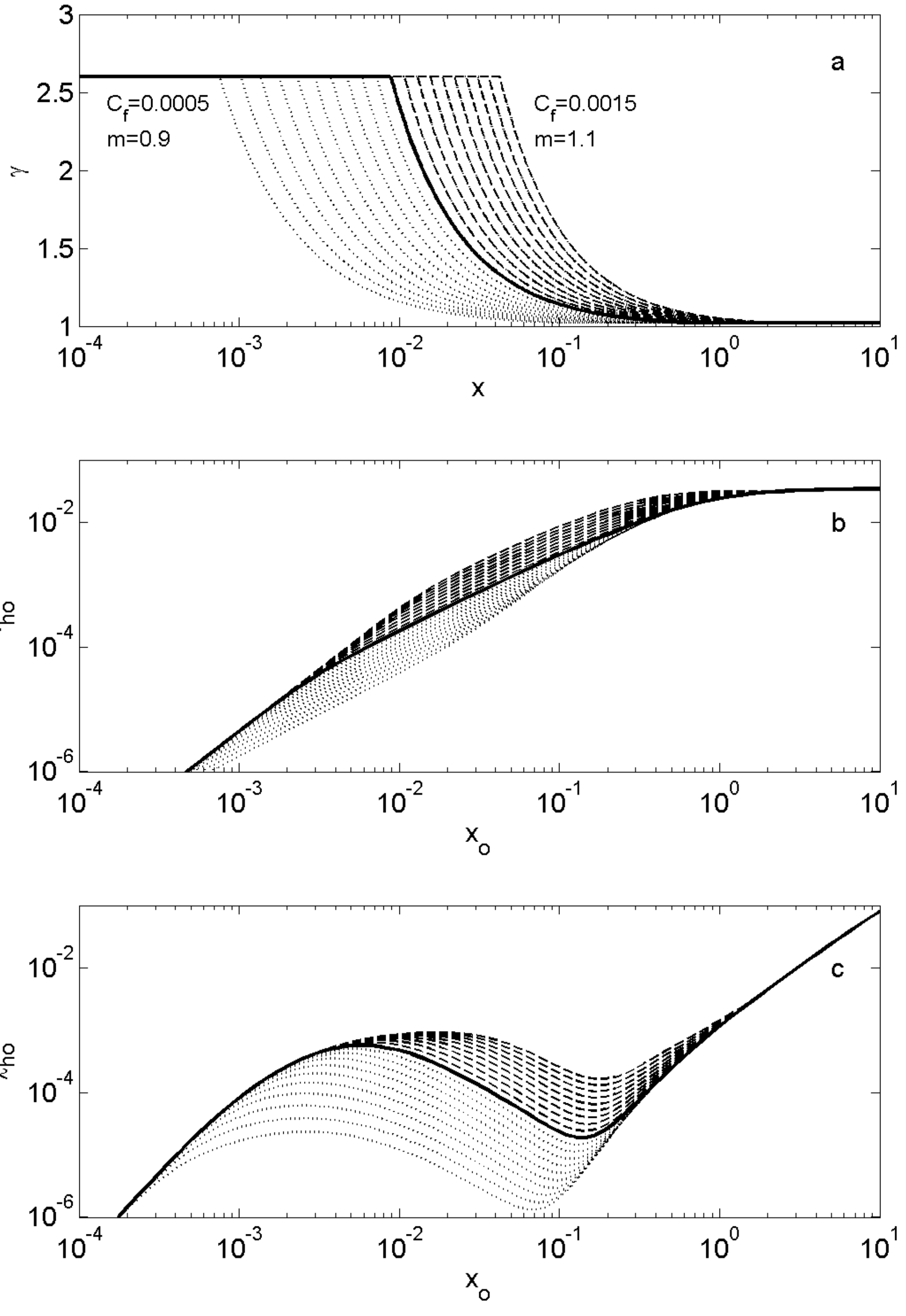

Fig 4.

n:\mat5work\sizescatter\floc\model_avesized2_b.m

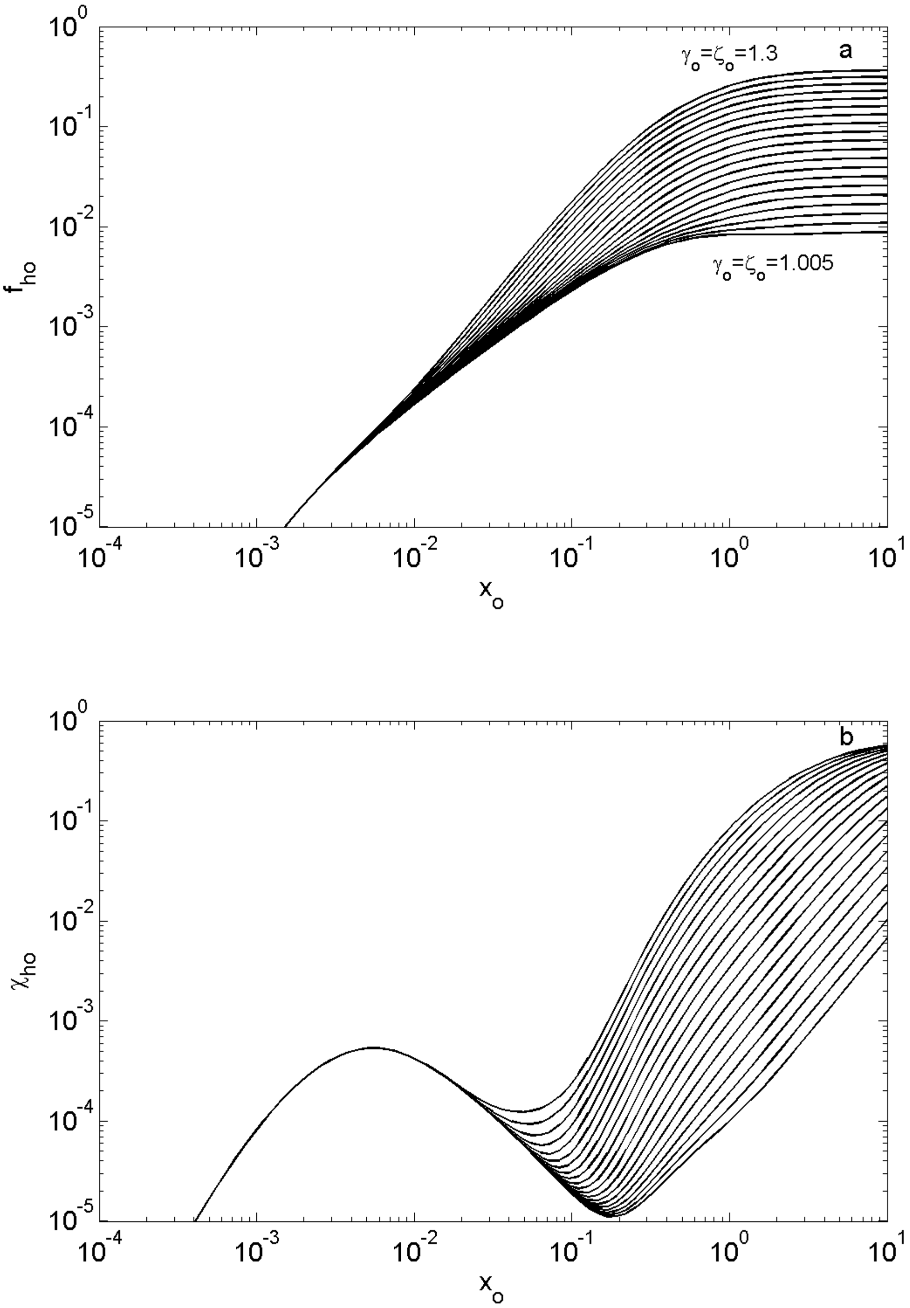

Fig 5.

n:\mat5work\sizescatter\floc\Iain_pdf1.m

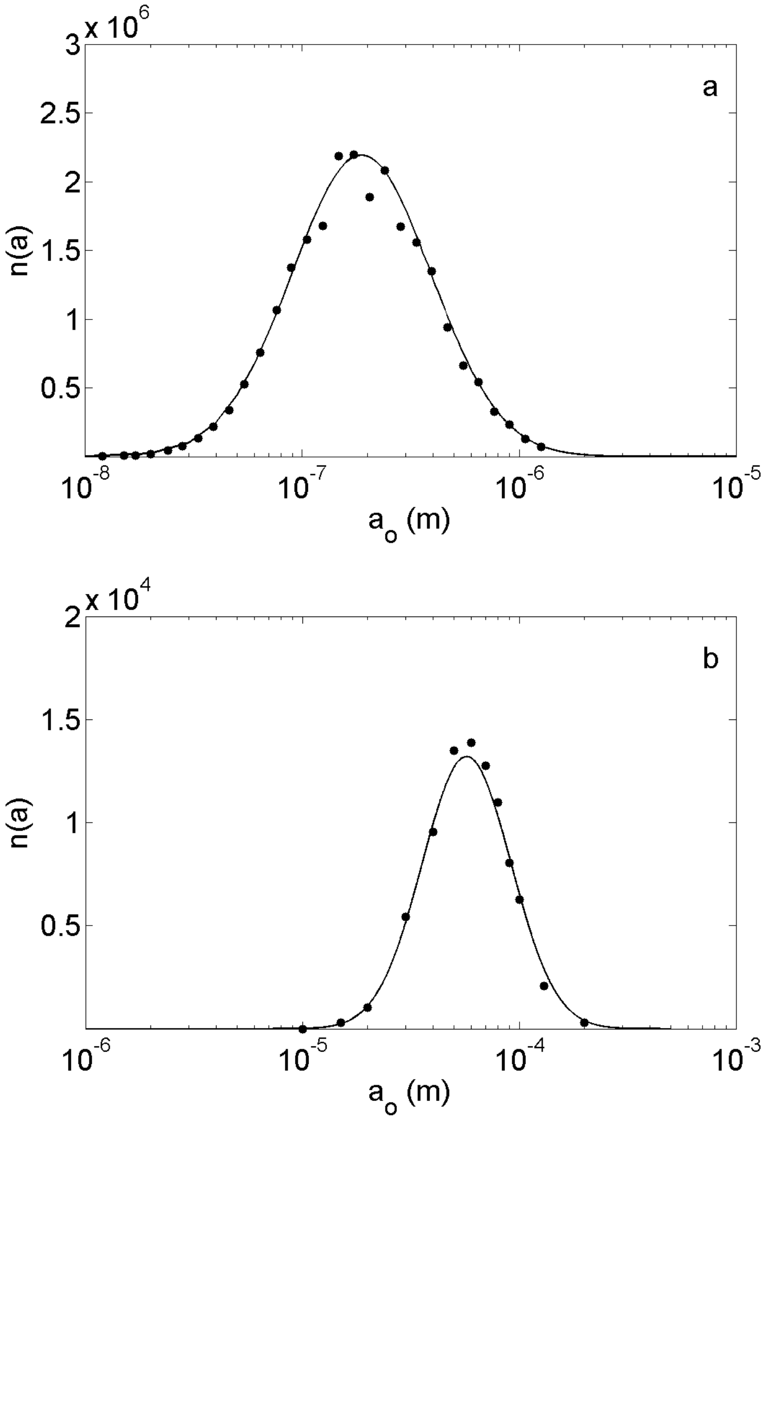

Fig 6.

n:\mat5work\sizescatter\floc\Iain_data_b.m

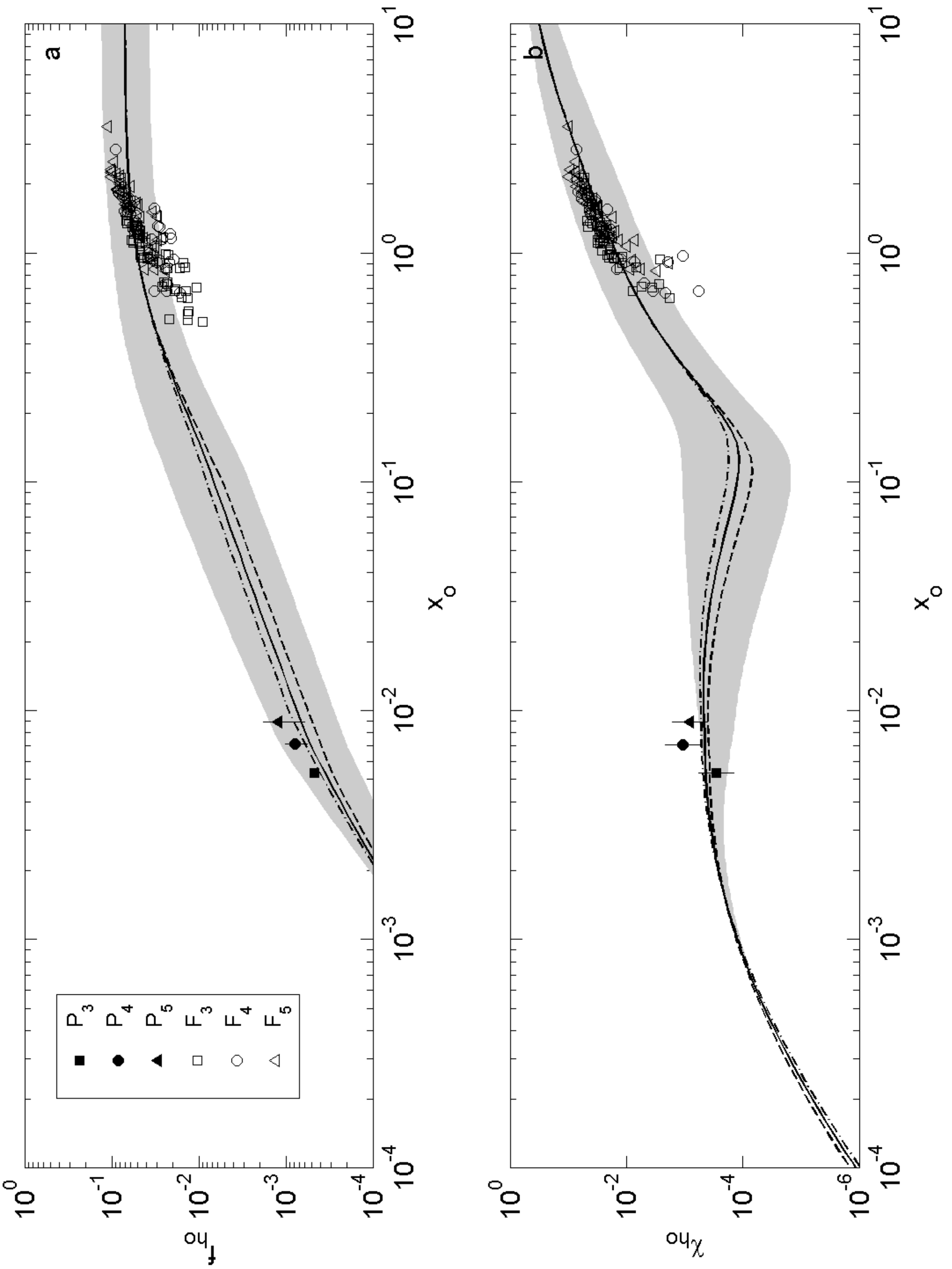

Fig 7